THE BELL SYSTEM TECHNICAL JOURNAL
Vol. 50, No. 8, October, 1971
Printed in U.S.A.

Optical Modulation at High Information Rates

By GERARD WHITE

(Manuscript received March 18, 1971)

This paper describes an optical modulation scheme with a demonstrated information rate of 1 Gb/s. The modulation scheme employs an electronic multiplexing technique to obtain the high data rate from four 250-Mb/s channels. Efficient interfacing between the gas laser beam and the high-speed electronic circuits is achieved using a traveling-wave type modulator structure. General considerations in optical modulation systems are also included.

I. INTRODUCTION

One of the major problems in engineering is that of interfacing between two differing technologies: This problem is particularly severe in laser communications systems where solid state electronics is to be interfaced with optics. It is, perhaps, at this technological interface that the early hopes of approaching the Shannon-Weaver information rates of laser systems have been limited. While electro-optic crystals have been shown to have modulation mechanisms operating in excess of 10 GHz[1] and photodetectors with gain-bandwidth products of the order of 100 GHz have been produced,[2] laser communications systems, so far, have demonstrated information rates significantly less than the capabilities of these components. Significant in the bandwidth limitation of demonstrated laser communications systems have been the demands on solid state circuit performance[3] imposed by the optical system and, in particular, the modulator. In this paper an optical modulation scheme is described in which system variations and subsystem configurations have been adopted in an attempt to relax the severe circuit performance requirements so that system information rate capabilities approach the bandwidth capabilities of the opto-electronic transducers. The system described, using an argon laser, has a demonstrated information rate of 1 Gb/s and some

techniques for improving upon this rate are proposed. Indicated system noise levels are observed to be low so that it may be possible to transmit a multilevel type code which could at least triple the information rate.

The paper, while describing state of the art results in wide-bandwidth optical communications, also provides tutorial matter in connection with general considerations in the system design and evaluation. The paper is divided basically into four sections, namely: (*i*) system considerations and optical arrangements, in which it is shown how variations in somewhat standard optical configurations can result in a high information rate modulation scheme; (*ii*) interfacing, which is mainly concerned with the producing of efficient interaction between the electronic circuits and the optical signals with traveling-wave type modulators; (*iii*) electronic circuits, which describes how the 1-Gb/s binary pulse code modulation (PCM) signals are generated by a gating and multiplexing process; and (*iv*) system performance, with general remarks on actual and extrapolated performance data.

II. SYSTEM CONSIDERATIONS

Various mechanisms exist for impressing information onto light beams including acousto-optic,[4] magneto-optic,[5] and electro-optic,[6] to mention but a few. Applied to laser beams, electro-optic interactions have proved most widespread, and in particular, the linear Pockels'[7] effect which is exhibited by many dielectric crystals. This effect relies on electric-field-induced perturbations of the natural birefringence of certain crystals including those in the point group 3m such as lithium niobate and lithium tantalate.[8] Lithium niobate's susceptibility to optically induced inhomogeneities to the natural birefringence[9] at relatively low optical beam powers makes its use as a modulator restricted and, in this application, lithium tantalate has been used. A figure of merit for $LiTaO_3$ when used as an electro-optic modulator is the half-wave voltage; this is the voltage required to induce a phase retardance of 180 degrees between components of the beam in the ordinary and extraordinary directions. Its value is derived from the elements r_{33} and r_{13} of the electro-optic tensor;[10] i.e.,

$$V_\pi = \frac{\lambda}{2(n_e^3 r_{33} - n_o^3 r_{13})} \cdot \left(\frac{c}{a}\right), \tag{1}$$

where n_o and n_e are the refractive indices experienced by ordinary and extraordinary components of the beam respectively. The factor c/a

is the inverse aspect ratio of the crystal, c and a being the width and length of the crystal respectively. For a value of wavelength equal to 496.6 nm, the half-wave voltage for $LiTaO_3$ is 2120 volts for the unity aspect ratio case. While large aspect ratio modulator rods can be prepared, so as to reduce the voltage required for a π-radian phase retardance, the value of voltage is still high enough to create severe performance demands on modulator driving circuitry in systems which rely on an "on-off" type modulator switch. Clearly, a partial modulation scheme will relax these standards but such a system is not easily implemented. It is pertinent at this point to consider some of the problems in realizing partial modulation schemes and at the same time discuss some of the advantages.

Consider the basic optical system shown in Fig. 1. It is easy to show that the modulated optical power, I_m, at the detector, is related to the applied modulator voltage V and the relative phase retardance ϕ of the beam components incident at the modulator by

$$I_m = \frac{I_i}{2}\left[1 - \cos\left(\phi + \frac{\pi}{2}\frac{V}{V_\pi} + \alpha\right)\right], \tag{2}$$

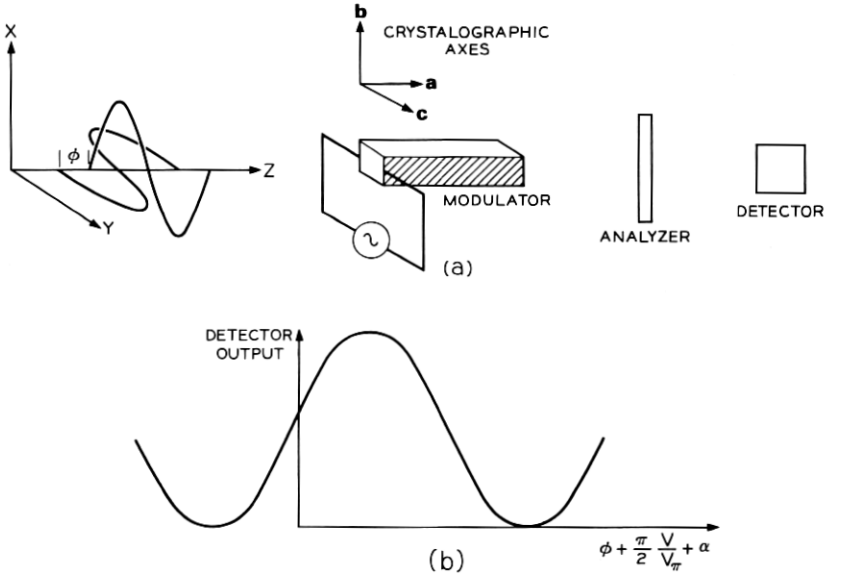

Fig. 1—(a) Basic optical modulation scheme. (b) System modulation characteristics.

where I_t is the total beam power at the modulator (assuming zero losses) and α is the retardation introduced by the natural birefringence of the crystal. Clearly, maximum beam modulation per unit modulation voltage is obtained when the x and the y components of the beam are equal in amplitude and adjusted for $\pi/2$ retardance at the analyzer. At this optimum bias and a crystal aspect ratio of 50 a small signal beam modulation depth of 8 percent per volt can be obtained. With such an arrangement satisfactory modulation depths of approximately 20 to 30 percent can be obtained with just a few volts of modulation potential.

In an actual system in which the modulated beam is detected via a photodetector which is coupled into a transmission structure of characteristic impedance Z_0, the system transfer function (defined as the differential ratio of modulation potential to potential appearing across the output transmission line) for a quasi small signal mode of operation is derived from equation (2) as

$$\frac{dV_{\text{out}}}{dV_{\text{in}}} = \frac{I_t}{V_\pi} \frac{\pi}{4} \frac{q\lambda}{hc} Z_0 \tag{3}$$

where q is the electronic charge, h is Planck's constant, and c is the velocity of light. The above relationship, based on the generation of one hole-electron pair per photon, assumes zero optical losses and a 100-percent quantum efficiency in the photodetector and works out to be approximately 0.5 per watt of beam power. Clearly, high beam powers will enhance the system transfer function coefficient, equation (3); however, a limit is imposed by optically induced inhomogeneities to the birefringence of the crystal. In an experimental system an upper limit of approximately 30 mW is realistic which gives a transfer function coefficient of 0.015 (not allowing for transmission losses) which for a modulation signal of several volts results in a satisfactory output amplitude. Satisfactory signal amplitude levels within the system, of course, depend on the system noise levels; in this respect, the presence of mode competition in a free-running laser system results in a very noisy channel. Two solutions to this problem are available: mode locking[11] and etalon tuning.[12] Mode locking effectively locks the longitudinal modes of the laser to produce a train of optical pulses at the frequency separation of the longitudinal modes, $c/2l$, where l is the length of the laser cavity. Optical communications systems incorporating mode-locked lasers offer some advantage and have been successfully demonstrated.[13,14] Mode-locked laser sys-

tems offer the availability of a stream of very narrow pulses of width inversely proportional to the oscillation bandwidth of the laser which can result in pulses of just a few picoseconds.[15]

A disadvantage of the mode-locked system is that optimum modulation depths and satisfactory base line definition are not compatible with low-voltage modulation since, in general, it is desirable in these systems to supply a modulation potential which is a substantial fraction of the half-wave retardation potential. One further disadvantage of mode-locked regime in gas lasers is the relatively low repetition rates of the optical pulses: This repetition rate is related to the frequency separation of the longitudinal modes, $c/2l$, and at short resonator spacings (required for high pulse repetition rates) the gain of gaseous lasers is insufficient to sustain oscillations. While techniques exist for effectively increasing this repetition rate by, for example, multiplexing[16] or harmonic pumping of the mode-locked frequency,[17] neither technique is a well established laboratory practice and the implementation of reasonably high rates (i.e., 1 GHz) is not, at present, conveniently realizable.

Relative noise immunity can be obtained with an etalon tuner by effectively selecting one pure optical frequency from the Gaussian line distribution. This is obtained by deforming the resonant poles of the laser so that only one conjugate pair lies within the laser gain curve.[18] The consequence of this type of operation is that mode competition is effectively eliminated and beam noise current is observed to be less than 5 percent of the total beam current. With such low noise powers, low modulation depths can be quite acceptable and a partial modulation scheme readily implemented.

There is no clear optimum in the choice of a particular optical frequency as a system carrier. While advantageous reductions in the modulator half-wave voltage can be obtained with shorter wavelengths [equation (1)], the quantum efficiency of the detector is in general reduced at these wavelengths (i.e., below 800 nm for Si). Focusing requirements are relaxed somewhat with shorter wavelengths since narrower diffraction-limited waists are obtained for a given far-field focusing angle. There is not, as yet, sufficient evidence for an optimum wavelength from the standpoint of optically induced changes to the birefringence. The absorption lines in $LiTaO_3$ are spaced such that, for gaseous laser output frequencies, the crystal is quite transparent and the choice of frequency is mainly determined by available powers from the various laser systems. In the system under discussion an ion

laser (argon) operating at 496 nm has been found convenient. This wavelength is somewhat below the characteristic peak in quantum efficiency for silicon photodetectors (800 nm), but nevertheless quantum efficiences of 0.3 A/W can still be obtained.

Coding for optical communications systems has so far received little attention. In the past the use of mode-locked lasers has given preference to a binary PCM coding technique. Recent studies[19] indicate that polarization multiplexed, phase shift keying, or pulse position modulation may be more appropriate to optical communications systems from a transmission standpoint. Problems still remain in implementing these modulation schemes. However, a frequency modulation scheme for space applications has recently been described[20] which shows promise for potentially wide bandwidths. Because of the advantages of regeneration, PCM systems appear attractive and in low-noise channels multilevel systems can be considered. The present system uses a binary type PCM coding scheme but is readily adaptable to multilevel with little increase in complexity.

III. OPTICAL ARRANGEMENTS

The optical arrangement used is of a fairly conventional nature employing a type of Senarmont compensator[21] as shown in Fig. 2. The argon laser provides a single frequency output of approximately 30 mW, plane polarized in the vertical direction. It is easy to show that a necessary condition for achieving optimum modulation is that the beam be circularly polarized at the analyzer plate. The consequence of a left- or right-hand polarization state is merely to induce a 180-degree phase inversion of the detected electrical signal. The circularly polarized state can be obtained by ensuring that the ordinary and extraordinary beam component amplitudes are equal with the necessary relative phase retardance. This is achieved by a 45-degree setting of the quarter-wave plate with an incident beam plane polarized at an angle $\theta/2$ which is adjusted by the half-wave retarda-

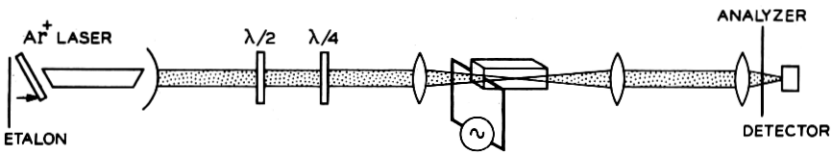

Fig. 2—Standard optical system with Senarmont type compensation.

tion plate. This particular arrangement can be easily checked by reference to the Poincaré-sphere.[22] Under these conditions, the x and y components of the beam are given by:

$$\left.\begin{aligned} E_x &= \sqrt{2}\ A\ \mathrm{Sin}\left(\frac{ct}{\lambda} - \frac{\theta}{2}\right) \\ E_y &= \sqrt{2}\ A\ \mathrm{Sin}\left(\frac{ct}{\lambda} + \frac{\theta}{2}\right) \end{aligned}\right\}. \tag{4}$$

The exact angle, $\theta/2$, is selected to compensate for the natural birefringence of the $LiTaO_3$ crystal. The electric-field-induced perturbations of the natural birefringence of the modulator rod translate to perturbations of the relative phase retardation of the x and y components of the exiting beam to produce a modulation of the beam ellipticity state. Collimation of the beam is provided to permit distant transmission. The analyzer may be placed before or after collimation depending on whether it is desired to transmit amplitude or polarization state modulation. At the receiver the beam modulation is converted to an electrical signal via the silicon avalanche photodetector. The avalanching mechanism provides a signal gain of only 2 or 3 due to the high optical power levels. In a detector operating at low levels, resulting from, for example, atmospheric attenuation of the beam, much higher gains should be possible. This is a desirable feature of the avalanche detector in that it provides a self-limiting or automatic gain control on the signal.

Efficient focusing of the beam for low-loss transmission through the modulator crystal is important. The problem can be dealt with in a number of ways and one method is given by Kogelnik and Li[23] in terms of the confocal parameters for optimum clearance. Another approach is to consider the percent transmission of power through the rod. Consider a rod of circular cross section, as shown in Fig. 3a, with an incident Gaussian beam with field distribution given by

$$E = E_0 e^{-[(x^2+y^2)/w^2]}, \tag{5}$$

where w is the width of the beam at the $1/e$ points. The intensity distribution, I, is therefore given by

$$I = I_0 e^{-2[(x^2+y^2)/w^2]}. \tag{6}$$

The total power in the beam, I_t, is computed from

$$I_t = I_0 \int_{-\infty}^{+\infty} \int_{-\infty}^{+\infty} e^{-2[(x^2+y^2)/w^2]}\, dx\, dy, \tag{7}$$

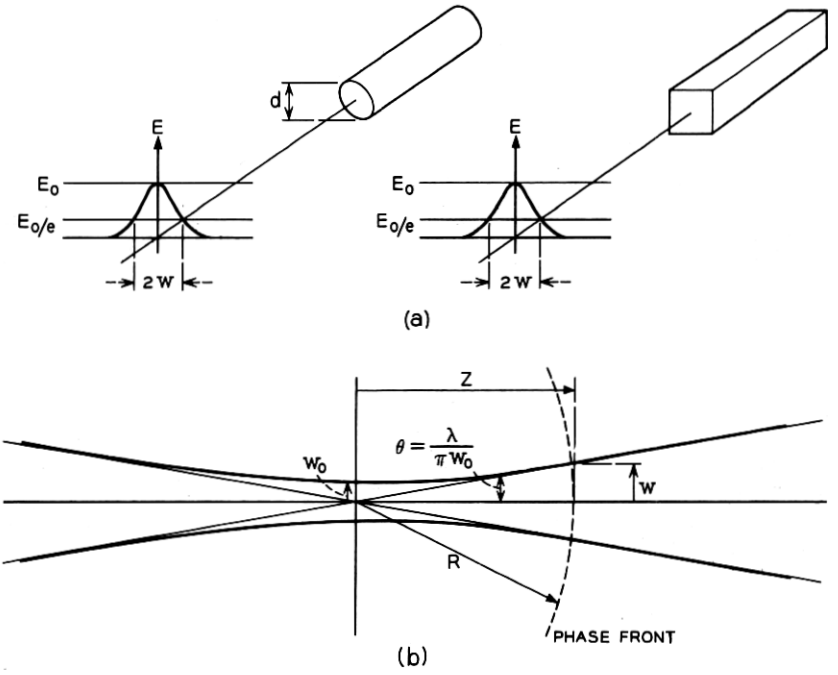

Fig. 3—(a) Modulator configurations. (b) Diffraction-limited beam waist.

which reduces to

$$I_t = \frac{I_0 \pi w^2}{2}. \tag{8}$$

Now, for the case of the circular cross section rod we can compute the rod dimension for 99-percent power transmission from

$$0.99\left(\frac{I_0 \pi w^2}{2}\right) = I_0 \int_0^{d/2} e^{-2r^2/w^2} 2\pi r \, dr, \tag{9}$$

which, after a parametric substitution, reduces to

$$\frac{d}{2} = 1.5w. \tag{10}$$

In a similar manner, the more practical case of a square cross section rod (Fig. 3a) can be dealt with, i.e.,

$$0.99\left(\frac{I_0\pi w^2}{2}\right) = I_0 \int_{-a}^{+a} \int_{-a}^{+a} e^{-2[(x^2+y^2)/w^2]}\, dx\, dy, \tag{11}$$

which, again after a parametric substitution, reduces to

$$a = 1.37w. \tag{12}$$

Clearly, the circular structure is more efficient from the standpoint of power transmission; however, the practical problem of applying uniform transverse electric field prohibits its use.

In matching the optical beam to the modulator rod, most power loss, due to dimensional limitations, will take place at the faces of the modulator due to beam expansion. Kogelnik has analyzed the expansion of focused Gaussian beams in some detail.[24] Figure 3b shows a typical beam waist at the focus point. The equations governing the beam parameters in this diffraction-limited case are:

$$w_0 = \frac{\lambda}{\pi\theta}, \tag{13}$$

where θ is the far-field diffraction angle;

$$w(z) = w_0\left[1 + \left(\frac{\lambda z}{\pi w_0^2}\right)^2\right]^{\frac{1}{2}}; \tag{14}$$

and

$$R(z) = z\left[1 + \left(\frac{\pi w_0^2}{\lambda z}\right)\right], \tag{15}$$

from which the confocal parameter, b, is obtained as the distance from the phase front radii minima as

$$b = \frac{2\lambda}{\pi\theta^2}. \tag{16}$$

The beam expansion can be completely specified, for a given wavelength, in terms of far-field diffraction angle, θ, which is, of course, the focusing cone half angle. For the case of a collimated beam† incident on the lens, θ is given by

$$\theta = \frac{w}{f} \text{ radians},$$

where w is the beam radius at the lens and f is the lens focal length.

† The description "collimated," within the context of Gaussian optics, here means a beam wavefront radius much greater than the focal length of the lens.

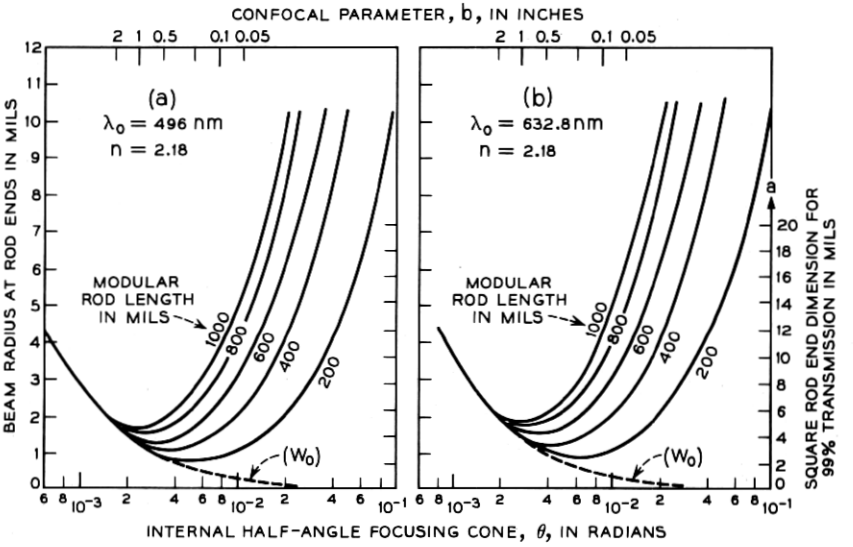

Fig. 4—Beam width of a modulator ends as a function of focusing cone angle: (a) $\lambda_0 = 496$ nm; (b) $\lambda_0 = 632.8$ nm.

Equation (14) may be used to calculate the beam radius at faces of a rod of length L for a given θ. This has been done for the case of $\lambda = 496$ nm and $\lambda = 632.8$ nm and the results are presented in Figs. 4a and b respectively. For each modulator rod length, a clear optimum cone angle is indicated. This optimum angle gives the same confocal parameter (on the upper abscissa) as Kogelnik's analysis. The ordinate on the right gives the necessary rod cross section for 99-percent optical power transmission in accordance with equation (12). Even for the case of the 1-inch rod with an aspect ratio of 100, a wide range of focusing cone angles are permitted for a high optical power transmission. In practical cases, criteria for high-efficiency transmission through the rod are easily met and other criteria assume importance. It is interesting to note that the curves for clearance in Figs. 4a and b coalesce for all rod lengths at a cone angle less than 1.5 milliradians. Thus, in this case, the transmission of optical power becomes relatively independent of the rod length.

One other criterion important in beam matching is that of nonuniqueness in the beam polarization state across the width of the beam. This arises as a result of the differing path lengths experienced by the various portions of the beam in the rod. Consider the wavefront

diagram shown in Fig. 5a. The optical path length of a particular portion of the beam in the modulator can be determined by a count of the wavefronts. Clearly, the path lengths are longer for the extremities of the beam than for the center. This is of no import in an isotropic media but in a crystal exhibiting birefringence, the result is a nonunique polarization state across the section of the beam. The problem of the propagation of Gaussian beams in anisotropic media has been analyzed in some detail[25] but it is sufficient here to adopt a somewhat simplistic argument to assess the quantitative effects of the nonuniqueness. The effect is important since it is at its maximum where the wavefront radius is at its minimum, i.e., when the length of the rod is equal to the confocal parameter, b. Consider the

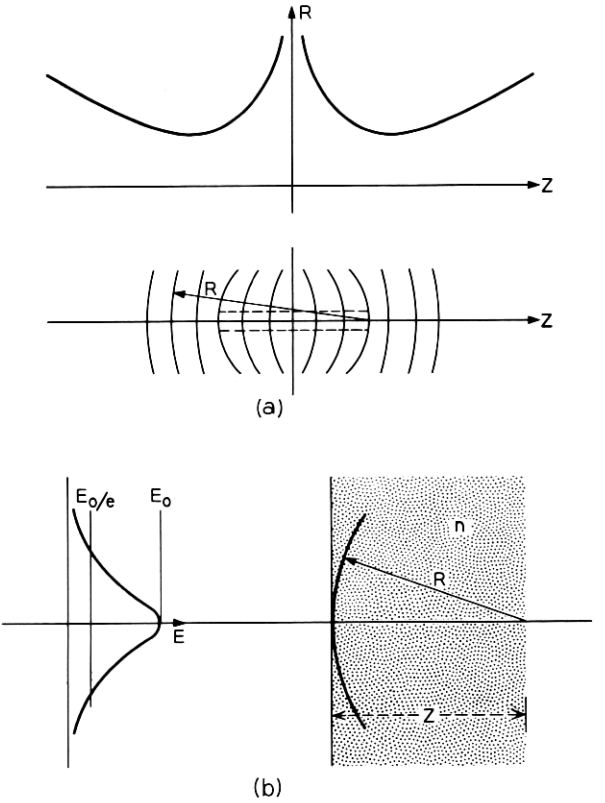

Fig. 5—(a) Wavefront radii at beam waist point. (b) Gaussian beam at surface of anisotropic media.

Gaussian beam incident at a flat face modulator crystal of length L as shown in Fig. 5b. The radius of curvature of the wavefront at the face of the crystal is given by

$$R(L/2) = \frac{L}{2}\left[1 + \left(\frac{\pi w_0^2}{\lambda L/2}\right)^2\right]. \tag{17}$$

For the important case of the rod length equal to the confocal parameter, for optimum clearance, equation (17) reduces to

$$R(L/2) = \frac{L}{2}\left[1 + \left(\frac{b}{L}\right)^2\right] = L. \tag{18}$$

A quantitative measurement of the nonunique polarization state of the beam can be obtained by determining the differences in relative phase retardation between the center and the E_0/e points of the beam. The radius of the beam at the face of the crystal is determined from

$$W\left(\frac{L}{2}\right) = W_0\left[1 + \left(\frac{\lambda L/2}{\pi w_0^2}\right)^2\right]^{\frac{1}{2}}, \tag{19}$$

which reduces to

$$W\left(\frac{L}{2}\right) = \sqrt{\frac{\lambda L}{\pi}} \tag{20}$$

for the confocal case.

The construction shown in Fig. 6a is useful in determining the nonuniqueness of polarization state for the above case. The situation is more complicated than that suggested by this simple construction in that the radius, R, is dependent on the beam polarization state as is

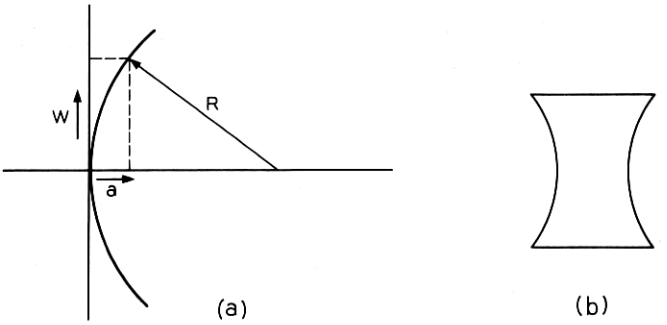

Fig. 6—(a) Evaluation of nonuniqueness in beam polarization state. (b) Modified modulator cross section to compensate for crystal birefringence.

also the beam angle in the crystal. Nevertheless, an approximation to the excess distance experienced by the E_0/e points of the beam is represented by the distance, a. The distance a is given by

$$a = R\left[1 - (\sqrt{1 - w^2/R^2})\right], \tag{21}$$

which, for $w/R \ll 1$ reduces to

$$a = \frac{w^2}{2R}. \tag{22}$$

Substituting equations (18) and (22) results in

$$a = \frac{\lambda}{2\pi} \tag{23}$$

and the relative differential path length, Δa, resulting from this excess distance is

$$\Delta a = \frac{\lambda}{\pi}(n_e - n_o) \tag{24}$$

(the effect is doubled due to the summation of the input and output excess distances). For $LiTaO_3$ this amounts to only 0.0004 λ, a negligible phase retardance. For other materials, such as $LiNbO_3$ or, more particularly, deuterated KDP, the effect will be much stronger due to the increase in the $(n_e - n_o)$ factor. The effect is analogous, in effect, to a built-in electric field, and where the polarization non-uniqueness is degrading, a modified cross section (Fig. 6b) can be adopted so as to produce a compensating nonlinear electric field across the modulator rod.

Of more practical significance in matching the beam to the modulator structure is the peak power intensity produced at the diffraction-limited beam waist which can give rise to optically induced inhomogeneities of the natural birefringence.[9] A field annealing process can reduce this susceptability[26] so that peak power intensities of 500 W/cm^2 are tolerable. The peak power intensity as a function of focusing cone angle is given in Fig. 7. This power intensity is obtained by combining equations (8) and (13) to give

$$I_0 = \frac{2n^2\pi\theta^2}{\lambda_0} \text{ W/cm}^2, \tag{25}$$

where θ is the internal focusing cone half angle. The strong dependence of power intensity on cone angle dictates a large confocal length, consistent with satisfactory clearance. A safety factor on clearance

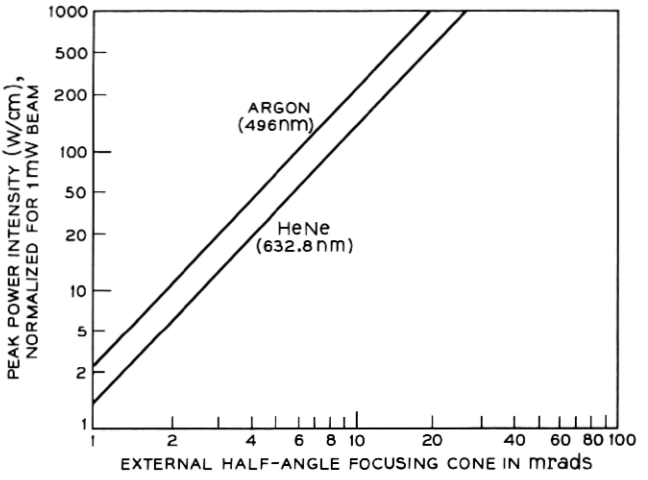

Fig. 7—Peak power intensity as a function of beam focusing angle.

has been proposed[6] which, in general, will restrict the minimum cone angle to some value less than the theoretical optimum indicated in Figs. 4a and b. For modulator rods of 10 × 10 mils cross section an internal half cone angle of 1.5 milliradians provides adequate clearance whilst maintaining satisfactory power intensities with beam powers of approximately 30 mW.

In summary, the matching of the beam to the modulator crystal is influenced by three criteria, viz.

(*i*) High-efficiency optical power transmission
(*ii*) Uniqueness of beam polarization state
(*iii*) Limitation of peak optical power intensity at the beam waist.

Separate optimization of items *i* and *ii* give rise to directly conflicting matching conditions. Fortunately, the degree of nonuniqueness of polarization state is not significant, for $LiTaO_3$, even for the worst case condition when the confocal parameter b equals the modulator rod length L. Further, the optimum exhibited for efficient optical power transmission is weak, and a wide range of focusing cone angles is allowable for very high efficiencies. Dominant in practical systems employing $LiTaO_3$ is the peak power intensity which will compromise the optimum condition for high power transmission. In cases when it is not possible to satisfy item *iii* and simultaneously maintain high-efficiency optical clearance, the crystal may be operated at an ele-

vated temperature (107°C) where the effect of optically induced birefringence changes is observed to relax at a rate faster than its creation.[9]

IV. INTERFACING—MODULATORS

Efficient interfacing of solid state circuitry with the electro-optic modulator is vital for high information capacity optical communications systems. In a practical system, the interfacing problem reduces to matching a transverse Pockels' effect crystal (lithium tantalate) to the impedance environment of the silicon driving circuits to achieve an efficient transfer of information onto the optical beam. A common approach in the past has been to regard the modulator as a lumped parameter structure which presents a reactive driving point impedance.[27,28] The major disadvantage of this approach is that not only must electrical charge be injected into the structure, but it must also be withdrawn by the driving circuits to restore the modulation field to its initial state. To accomplish this charging and discharging, at high data rates, impractically large charging and discharging currents are necessary. Further, the capacitive load will create a mismatch in the driver-modulator transmission path resulting in standing waves with consequent modification of the impressed waveform.

A different approach is to make use of the intrinsic characteristic impedance of approximately 55 ohms which is exhibited by $LiTaO_3$. This impedance can be realized by rearranging the modulator structure to make use of the inherent distributed parameter structure of the modulator crystal. The resulting modulator will be of the traveling-wave type,[29,30] which presents a real driving point impedance so that an efficient interface is obtained with the impedance levels of high-speed silicon transistor circuits (50 ohms). Previously traveling-wave type interactions have been adopted to increase the modulator bandwidth;[31] however, in this application their primary use is to provide improved impedance matching. The improved bandwidth appears as a secondary effect as will be discussed later.

The exact characteristic impedance of the modulator structure can be determined from the differential capacitance and inductance along the length of the crystal. The capacitance per unit length is simply

$$C = \epsilon_0 \epsilon_r \frac{b}{c} \text{ F/m}, \tag{26}$$

where b and c are the crystal dimensions along the **b** and **c** optical

axes respectively. This, of course, assumes zero fringing of the electric field outside the crystal which is justifiable since $\epsilon_r \gg 1$. The inductance L due to the two parallel crystal electrodes of length ℓ is[32]

$$L = 4\ell\left[\log_e \frac{2\ell}{b} - \log_e \frac{2\ell}{c} + 1.5 - \log_e e + \log_e k - \frac{c}{\ell} - \frac{1}{4}\frac{c^2}{\ell}\right], \quad (27)$$

where $\log_e e$ and $\log_e k$ are functions of b and c given in Ref. 32. For a modulator crystal of 10 mils square cross section, the inductance per unit length reduces to

$$\frac{dL}{d\ell} = \left(6.3 - \frac{c^2}{\ell^2}\right) \text{nH/cm}. \quad (28)$$

So that, combining (26) and (28), the characteristic impedance, as a function of distance, is

$$Z_0(\ell) = \sqrt{\frac{\left(6.3 - \frac{c^2}{\ell^2}\right)c}{\epsilon_0\epsilon_r b \times 10^2}} = 41 \text{ ohms} \quad (29)$$

for $c^2 \ll \ell^2$, i.e., at some distance from the ends of the modulator. The exact variation of characteristic impedance along the length of the rod is given in Fig. 8. The deviations of Z_0 at the rod ends are in fact abstractions, which will not be exhibited by a practical structure due to the presence of connections to the electrode end points which results in a more complex situation. It is assumed in this calculation that there is no dispersion of the dielectric permittivity. Experimental high-frequency measurements have indicated that this is the case[33] and further experiments have extended this result to 6 GHz.[34]

The group velocity differences of the electrical and optical signal velocities in the modulator will give rise to a bandwidth limitation. This limitation is readily analyzed by consideration of the situation depicted in Fig. 9. The voltage experienced by an optical wave at a point z in the modulator rod is

$$V(z) = V \operatorname{Sin}\left[\omega\left(t + \frac{z}{v_\ell} - \frac{z}{v_e}\right)\right], \quad (30)$$

where v_ℓ and v_e are the velocities of the light and electrical signals respectively in the modulator rod. For a rod length, L, the total induced phase retardation of the optical beam is, therefore,

$$\phi_{\text{Tot}} = \int_{-L/2}^{+L/2} \frac{\pi V}{V_\pi L} \operatorname{Sin}\omega\left(t + \frac{z}{v'}\right) dz, \quad (31)$$

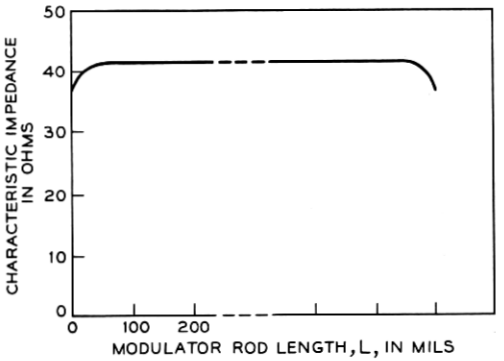

Fig. 8—Modulator characteristic impedance as a function of distance along crystal.

where

$$\frac{1}{\nu'} = \frac{1}{\nu_\ell} - \frac{1}{\nu_e}\,; \tag{32}$$

hence,

$$\phi_{\text{Tot}} = \frac{2\pi V \nu'}{V_\pi L} \operatorname{Sin} \frac{\omega L}{2\nu'} \operatorname{Sin} \omega t \tag{33}$$

which is of the familiar form shown in Fig. 10a. This amplitude spectrum results in the Dirac response of Fig. 10b and the electro-optic transfer function step function response time is, therefore,

$$t_r = L\left[\frac{1}{\nu_e} - \frac{1}{\nu_\ell}\right]. \tag{34}$$

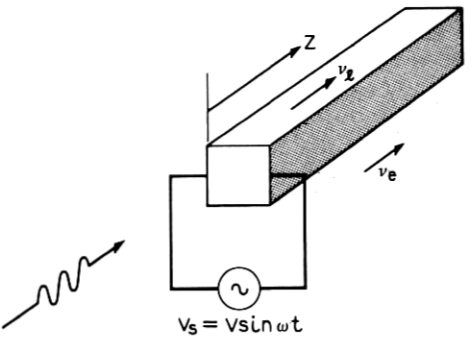

Fig. 9—Traveling-wave type modulator structure.

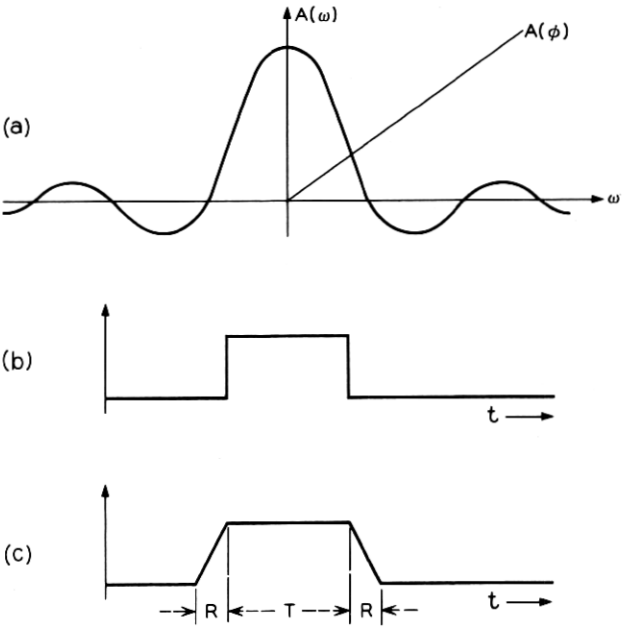

Fig. 10—(a) Amplitude spectrum of traveling-wave modulator. (b) Dirac response. (c)System response to pulse width T.

Typically, for a 1-cm-long modulator crystal a rise time of 150 ps is indicated.

The modulator bandwidth can be increased with velocity compensation of the light and electrical signals. Kaminow, et al.,[35,36] and Peters[37] have described some techniques for accomplishing this type of compensation. The proposals suffer from some disadvantages in practical realizations, including a loss of modulation power, fabrication problems in achieving high-efficiency power transmission, and, in particular, the latter proposal[37] could result in multimode propagation of the electrical modulation signal in the modulator structure. In practice, the modulator bandwidth limitation is not significant, with respect to system bandwidth, even in high information rate systems (1 Gb/s) and it is not necessary to resort to velocity compensation techniques. This is easily shown by considering an input pulse, $f_1(t)$, of width T where $2T$ is the system information rate interval, i.e.,

$$f_1(t) = A[H(t) - H(t - T)], \tag{35}$$

denoting the unit step function as $H(t)$. The system Dirac response, $f_2(t)$, has been shown to be

$$f_2(t) = B[H(t) - H(t - R)], \tag{36}$$

where

$$R = \frac{L}{C}(\epsilon_r^{\frac{1}{2}} - n). \tag{37}$$

The system response, $f_0(t)$, to $f_1(t)$ is given by the convolution

$$\begin{aligned} f_0(t) &= f_1(t) * f_2(t) \\ &= \int_0^t A[H(\tau) - H(\tau - T)]B[H(t - \tau) - H(t - R - \tau)]\, d\tau \end{aligned} \tag{38}$$

from which it is obvious, from the graphical form of the convolution integral, that $f_0(t)$ is as shown in Fig. 10c. So that, providing $R \leqq T/2$ the modulator bandwidth is not limiting; this is clearly so at information rates of 1 Gb/s.

It is important to observe from (33) and (34) that a trade off exists between modulator bandwidth and half-wave voltages so that it is possible to employ velocity compensation to permit longer crystals (while maintaining the same bandwidth as the uncompensated structure) to achieve advantageous reduction in the half-wave voltage. This trade off is also possible with different modulator materials. In fact, a gain-bandwidth product can be assigned to a particular modulator material. With this figure of merit, the gain is related to the inverse half-wave retardation voltage and the bandwidth is related to the optical refractive index and the microwave dielectric permittivity, i.e.,

$$GB = \frac{1}{(n - \epsilon_r^{\frac{1}{2}})V_\pi}. \tag{39}$$

This figure of merit is given for a number of modulator materials in Table I. The situation is more complex, however, than is suggested by a numeric value of the gain-bandwidth product: GaAs, for example, only exhibits below bandgap transmission for $\lambda > 900$ nm and GaP incorporates a dielectric relaxation time which can be as large as 10 μs.[38] Further, the mechanical properties of the materials dictate the feasibility of fabrication of large aspect ratio crystals to effect a gain-bandwidth trade off. Other factors, including free carrier optical absorption and optically induced crystal damage, further complicate the choice of material.

TABLE I — FIGURE OF MERIT FOR DIFFERENT MODULATOR MATERIALS

Material	Type	n(av)	ϵ_r	V_π†	$GB(V^{-1} \times 10^{-5})$
$LiTaO_3$	Ferroelectric Perovskite	2.18	43	2130	10.7
$LiNbO_3$	Ferroelectric Perovskite	2.25	30	2340	13.3
KH_2PO_4	KDP[40]	1.5	21	4350	7.5
GaAs	AB-Type Semiconductor	3.5	12.5	3870	$\rightarrow \infty$
GaP	AB-Type Semiconductor	3.45[39]	11.1[38]	7830	$\rightarrow \infty$

† Extrapolated to $\lambda = 496$ nm.

$LiTaO_3$ represents a compromise of the gain-bandwidth product and the other factors while still providing significant advantages in response time when incorporated in a traveling-wave structure compared to the lumped parameter configuration. Equation (34) can be used to compare the performance of the traveling-wave $LiTaO_3$ modulator with the electro-optic transfer function rise times obtainable with lumped parameter configurations operating in the normal 50-ohm environment. The rise times are, of course, a function of modulator rod length as is seen in Fig. 11. Even for the double-pass-type lumped parameter structure,[13] the response times of the uncompensated traveling-wave structure are significantly superior. Typically, for a modulator rod length of 500 mils, the rise times are 150 ps, 250 ps, and 500 ps for the traveling-wave, double-pass lumped parameter, and single-pass lumped parameter structures respectively.

The traveling-wave modulator structure has been realized in microstrip thin film form on an alumina (Al_2O_3) substrate as shown in Fig. 12. The alumina substrate has microstrip transmission lines of 50 ohms characteristic impedance etched in the evaporated chrome-gold layers with the reverse side metalization removed below the modulator rod. Connections are brought through the substrate from the reverse side metalization to make contact with the upper contact lands. The modulator crystal has evaporated electrodes, typically chrome and palladium, on opposite faces along the longitudinal axis. Placement of the modulator crystal, with the b optical axis perpendicular to the surface of the substrate, is facilitated with low-temperature solder which also provides acoustic damping.[27] The electrical modulation signal is applied via the coaxial-to-strip-line transition, the strip line, and the rod, and exits from the substrate to be absorbed in a matching termination. The possibility exists, however, for reapplying the elec-

trical modulation signal to further cascaded modulator structures without the need for any additional electrical power. In this manner, not only can increased modulation depths be obtained but some degree of compensation can be obtained for the electrical and optical velocity differences by adjusting the relative electrical and optical delays between the two modulators as shown in Fig. 13.

A photograph of an actual modulator structure with a 500-mil-length rod is shown in Fig. 14. The time domain reflectometry (TDR) trace of the characteristic impedance throughout the modulator is presented in Fig. 15a. Small perturbations in characteristic impedance due to the coaxial-to-strip-line transitions are observed with a much larger deviation from the 50-ohm impedance level along the length of the crystal. The crystal impedance level ($\sim$ 30 ohms) is less than indicated by equation (29) and is partially attributable to the electric field deformation due to the close proximity of the high permittivity ($\epsilon_r = 9.7$) alumina substrate. The time resolution of the TDR system is 30 ps and the relative slowness of the drop to the 30-ohm level indicates the possibility of a dielectric relaxation mechanism in the crystal. The impedance mismatch results in a reflection coefficient, ρ, of 0.25 or a VSWR of only 1.65, and no significant deformations of

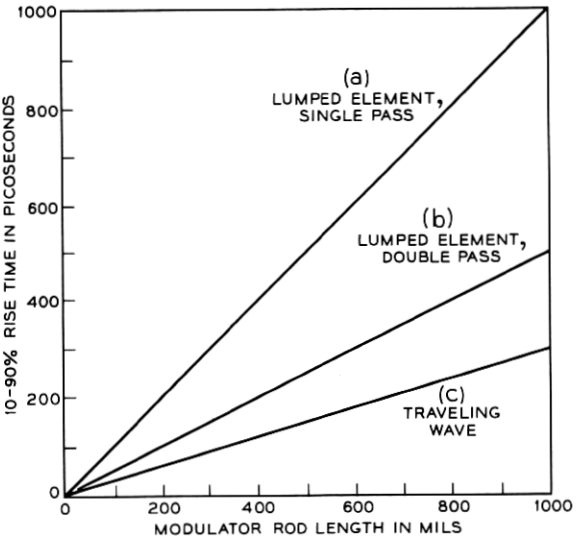

Fig. 11—Rise time as a function of modulator rod length for traveling-wave and lumped parameter single- and double-pass systems.

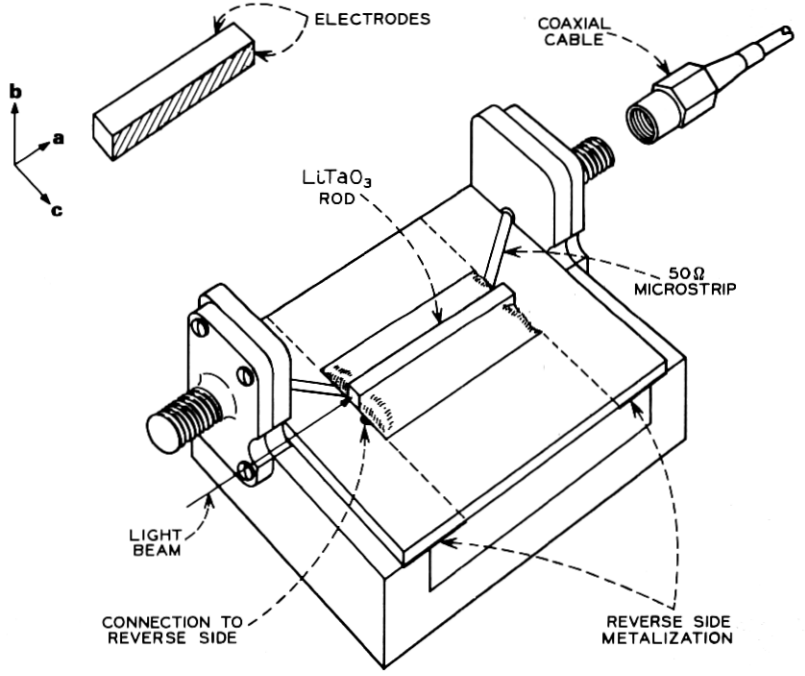

Fig. 12—Traveling-wave modulator embedded in microstrip transmission lines.

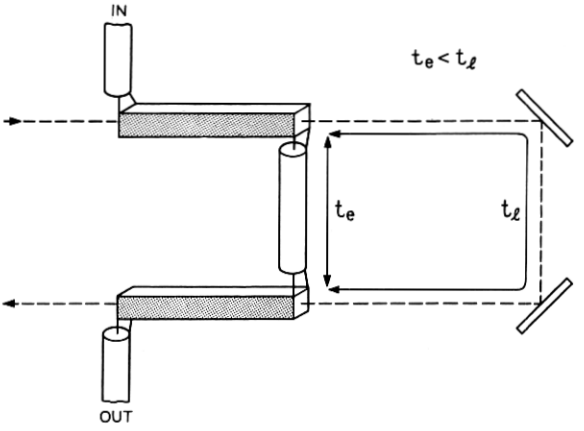

Fig. 13—Cascaded traveling-wave modulator structure.

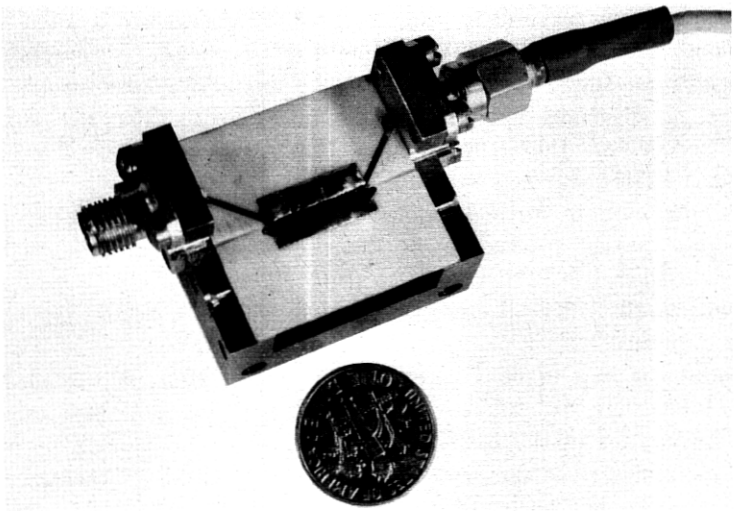

Fig. 14—Photograph of traveling-wave $LiTaO_3$ modulator.

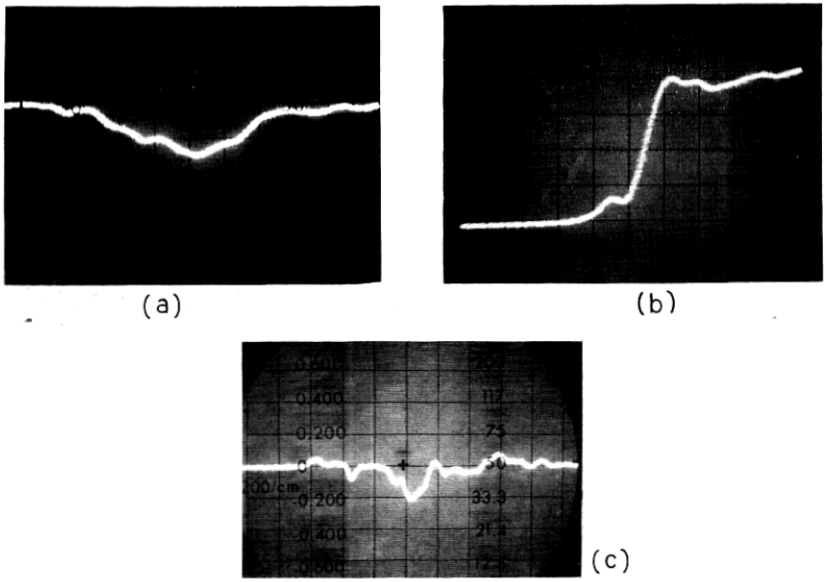

Fig. 15—(a) TDR characteristics for $LiTaO_3$ modulator (100 ps/cm). (b) Electrical pulse transmission through modulator (100 ps/cm). (c) TDR characteristics for $LiNbO_3$ modulator (200 ps/cm).

the modulation waveforms are observed in the actual system as a result of the nonunity VSWR. The high-frequency attenuation of the electrical signal after traversing the modulator structure is illustrated in the time domain response of Fig. 15b. The rise time is significantly less than 100 ps indicating an electrical band pass in excess of 4 GHz.

Lithium niobate, with a lower permittivity, produces a characteristic more nearly approximating the desired 50-ohm impedance level as indicated in the TDR trace of Fig. 15c. This is for a 360-mil-length rod with a 10 × 10-mil cross section mounted in a similar traveling-wave structure.

Modulator rods of 60:1 aspect ratios (10 × 10 × 600 mils) have been fabricated without any noticeable evidence of stress induced inhomogeneities to the birefringence and the actual system performance to be described employs this length of modulator crystal.

No attempt has been made to compensate for the strong temperature dependence of the electro-optic effect in $LiTaO_3$. Small signal modulation reduces this problem since RF heating is negligible. Optical power absorption and ambient temperature changes can be significant and in a practical system the cascaded, temperature compensated structure of Peters[41,42] can be employed. This scheme has recently been realized in a 10 × 10-mil cross section crystal in a traveling-wave type structure.[43]

V. HIGH-SPEED ELECTRONIC DRIVING CIRCUITS

At present, a major factor in restricting the information capacity of optical communications systems is the speed of operation of the electronic driving circuits. It is in this area that effort will result in information rate increases. The present system uses an electronic multiplexing and gating process to achieve the 1-Gb/s PCM word patterns necessary to produce the overall system information capacity. Optical multiplexing[16] has been proposed as a means of increasing system information capacity and it is possible that this multiplexing technology could complement the electronic multiplexing described here. Indeed, such a combination may be preferable to a wholly optical multiplexing scheme since the complexity of the optical arrangements would be reduced.

The general schema of the electronic PCM system is shown in Fig. 16. Here basic system timing is provided by a master 250-MHz sine-wave oscillator. After division by a quarter-wave transformer to

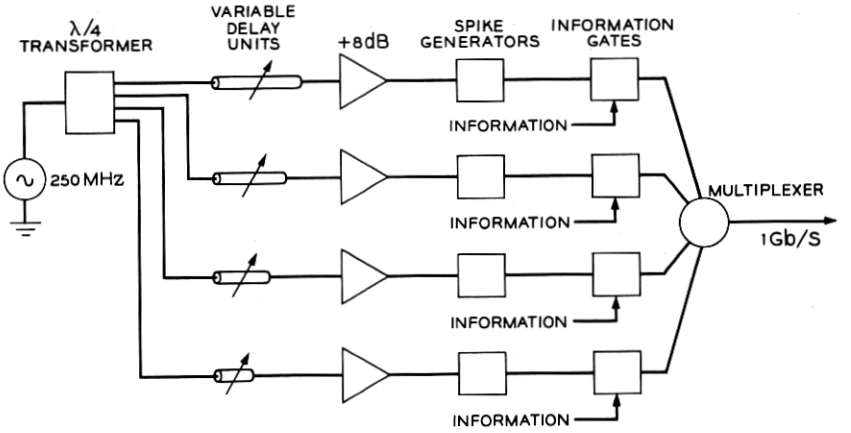

Fig. 16—Schema of electronic PCM system.

achieve impedance matching, the waveform provides system synchronization and drive to four Boff (snap-off) diode subnanosecond spike generators. Amplification and variable delay units are provided for adjustment of the phase and amplitude of the four channels. The amplifiers are standard class C tuned stages providing approximately 8 db of gain and the variable delay units are standard variable-length coaxial lines. The timing of the four waveforms is arranged so that the spike pulses fall in sequence into each of four time slots or windows, 1 ns wide. In this manner the pulses can be multiplexed in an OR gate multiplexer to produce a bit rate of 1 Gb/s. Information is impressed onto the pulse trains in the individual channels in "information AND gates." With this technique the information signals can be of a relatively slow nature (i.e., rise and fall times of 2 ns) at a bit rate of 250 Mb/s. Logic processing prior to impressing onto the spike trains is already available in standard emitter-coupled integrated circuit form.

The realization of some of the constituent parts of this system represents some difficult design and fabrication problems and it is pertinent to discuss in some detail these subsystem elements.

5.1 *Boff Diode Spike Generators*

The high-speed subnanosecond spikes are generated in a tuned circuit excited by the abrupt cessation of carrier storage in the Boff diode. The generator is of a conventional shunt-mode type which is well

documented.[44,45] The actual circuit form is shown in Fig. 17a. The width of the pulse is determined by the half period of the resonant circuit formed by L_t and C_t. L_m and C_m provide matching to the sine-wave source whilst R_b sets the dc bias.

Amplitudes of approximately 10 volts are obtained with pulse base widths of 700 ps. Significantly narrower pulse widths are easily obtainable with the promise of higher orders of multiplexing and concomitantly higher bit rates. The prime limiting factor to this type of extrapolation, however, is the transmission bandwidth of the information gate. A typical spike generator output waveform is shown in Fig. 17b. Figure 17c shows the output waveform of the four channels with the pulses positioned in their relative 1-ns time slots. The circuit is realized in conventional strip line construction with lumped parameter reactances.

5.2 *Information Gates*

The function of the information gate is to transmit or inhibit individual spike waveforms at a bit rate of 250 Mb/s in response to a "1" or a "0" on the information signal. High-speed considerations would normally suggest a passive gate employing Schottky barrier diodes; however, for the case of equal input and output impedance it is not possible to obtain a passive gate gain in excess of 0.5. In

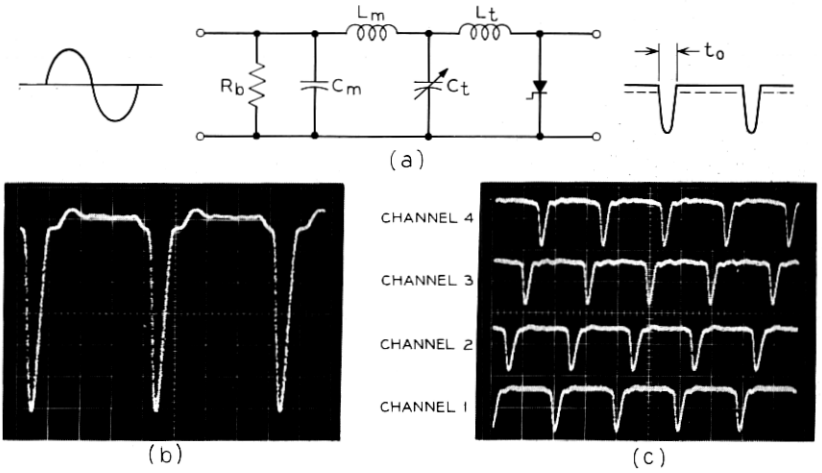

Fig. 17—(a) Boff diode spike generator. (b) Single-channel output waveform (1 ns/cm, 2 V/cm). (c) Four-channel output in relative time slots (2 ns/cm, 5 V/cm).

contrast, active gates can give gains in excess of unity although a more limiting bandwidth is imposed. The bandwidth limitation can be minimized to acceptable levels with the current routing pair configuration which has been used in this system. The simple circuit form is shown in Fig. 18a. The actual circuit incorporates a number of dc restoration networks so that little demand is made on the entropy of the information signal.

The high-speed spikes with frequency components in excess of 1 GHz are applied to the common emitter node via a terminating resistance resulting in current pulses with amplitudes of the order 100–200 mA. Current routing between transistors Q_1 and Q_2 is controlled by the base potential of Q_1 which is determined by the amplitude of the information signal. With this configuration Q_2 operates in essentially the common-base mode so that the full common-base current gain cutoff frequency of the device can be realized. In contrast, the switching action in response to the information pulses takes place

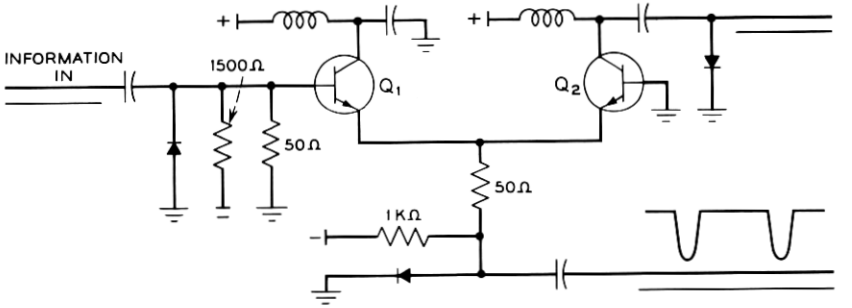

(a)

(b)

Fig. 18—(a) Information gate. (b) Information gate switching: top trace, output; bottom trace, information input (2 ns/cm, 2 V/cm).

at the base where switching speed is commensurate with the rise times of the information signal.

As a result of the large-amplitude currents being switched in the devices, high-level injection effects occur. The problem then is that phenomena, such as emitter crowding, transverse voltage drops[46] in the base, and the Kirk effect,[47] produce device parameter degradation. These high-level injection effects are still significant in the nine-stripe geometry devices used. Device parameter degradation has two effects, first, a bandwidth limitation which in turn produces a reduction in output pulse amplitude, and second, emitter-to-base voltages which become quite large so that complete current switching from one device to the other is not possible. A consequence of the latter effect is that it is not feasible to switch off Q_1 at any time (due to reverse emitter-base junction breakdown of Q_2), and Q_2 is only switched off in response to large (5 V) pulses at the base of Q_1. This degenerate switching mode of operation is satisfactory however, since only the output of Q_2 is utilized. The overall capabilities of the information gate are a switching time of less than 2 ns with transmission bandwidth in excess of 1 GHz for output pulse amplitudes of 7 volts. Typical switching action is indicated in Fig. 18b. Here, information impression on the spike pulse train is shown (upper trace) for a 10101 word pattern, in response to the relatively slow information signal (lower trace). It is to be noted that the base width of the exiting word pattern pulses is still significantly less than 1 ns so four-channel multiplexing is still efficient. The circuit is realized in thin film microstrip with thin film chrome resistors and beam leaded transistors. The actual structure is shown in Fig. 19. The devices used had a cutoff frequency of approximately 4 GHz and a collector-base capacitance of approximately 0.3 pF.

5.3 *1-Gb/s Multiplexing Gate*

Multiplexing of the four information bearing pulse trains can be accomplished with a four-input "OR" gate. "OR" gates, unlike "AND" gates, can have unity gain with passive components. The use of passive components relaxes somewhat the high-speed circuit requirements for the multiplexer. In particular, Schottky barrier diodes can be used to advantage for the multiplexer. The low carrier storage time of these devices permits the high-speed circuit performance required. The actual circuit used is a simple four-diode structure in microstrip as shown in Figs. 20a and b. This particular hybrid construction used leadless inverted device (LID) packaging of the devices.

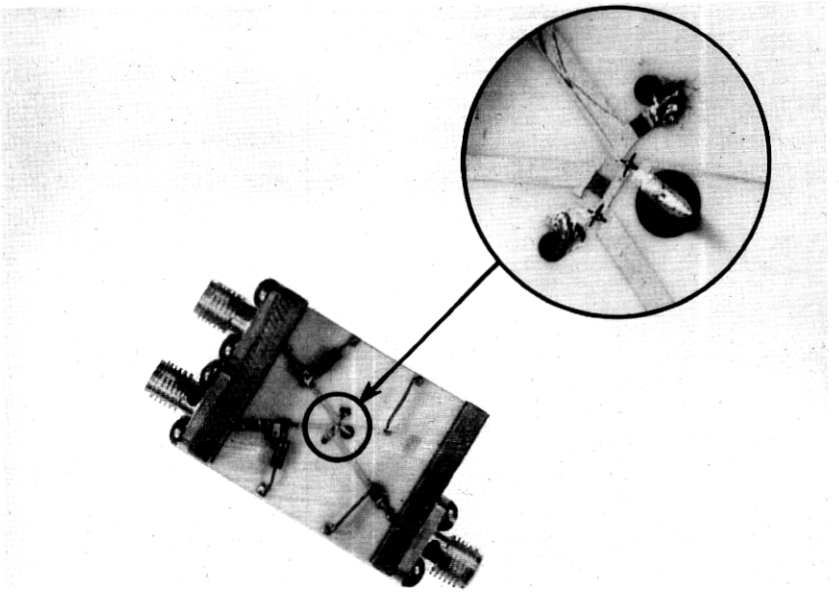

Fig. 19—Information gate realization in thin film microstrip with beam lead devices.

A typical set of input waveforms to the multiplexing gate is shown in Fig. 21a. Here, the four channels are positioned in their relative 1-ns-wide time slots with a 10101 word pattern on channel 1. The multiplexed, 1-Gb/s output is shown in Fig. 21b. Little degradation in wave form speed is apparent. The speed limiting factors are Schottky barrier diode storage time and junction capacitance. The former can be significantly less than 100 ps[48] and the latter can be a fraction of a picofarad.[49] In cases where a large number of channels are multiplexed, the junction capacitance can become the dominant limiting factor since it is a cumulative effect. Diode barrier potential and differential "on" resistance result in some amplitude attenuation which attenuates output pulses to 5 or 6 volts.

The output from the multiplexing gate is applied, via a coaxial line, to the $LiTaO_3$ traveling-wave modulator.

VI. OTHER REALIZATIONS

Other electronic realizations of the circuit functions described are possible which should provide improved performance at higher data rates with higher modulation depths. An example of an alternative

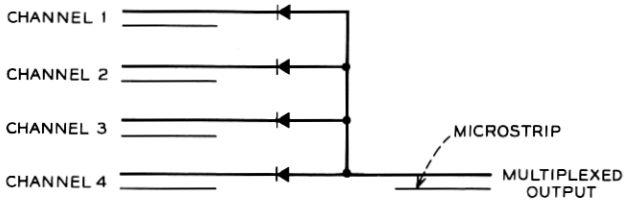

(a)

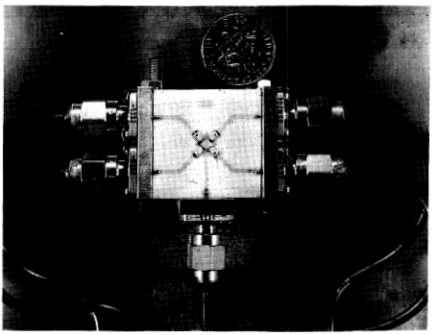

(b)

Fig. 20—(a) Multiplexing gate "OR" circuit. (b) Multiplexing gate realization in thin film microstrip.

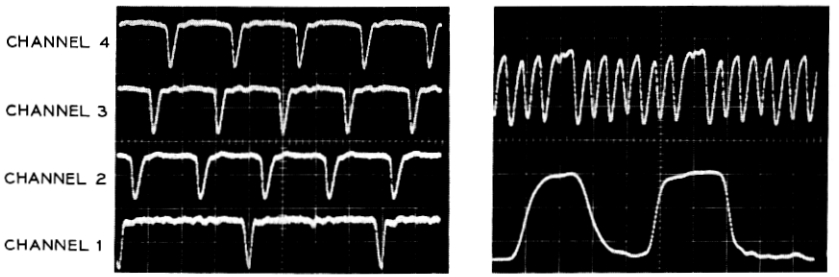

(a) (b)

Fig. 21—(a) Input waveforms to multiplexing gate (2 ns/cm, 5 V/cm). (b) Upper trace: 1-Gb/s multiplexed output; lower trace: channel 1 input word pattern (2 ns/cm, 2 V/cm).

realization is shown in Fig. 22. In this realization the functions of the information gates and the multiplexer are combined by taking advantage of inherent multiplexing capabilities of the collector output circuits. In this manner, attenuation resulting from the multiplexer diode barrier potential and differential "on" resistance is eliminated. High-level injection effects in the information gate devices can be reduced by cascaded structures so that significantly higher amplitude modulation waveforms can be obtained. Such realizations could lead to "on-off" systems with very high data rates (in excess of 1 Gb/s). The limiting factor in these realizations is the cumulative addition of

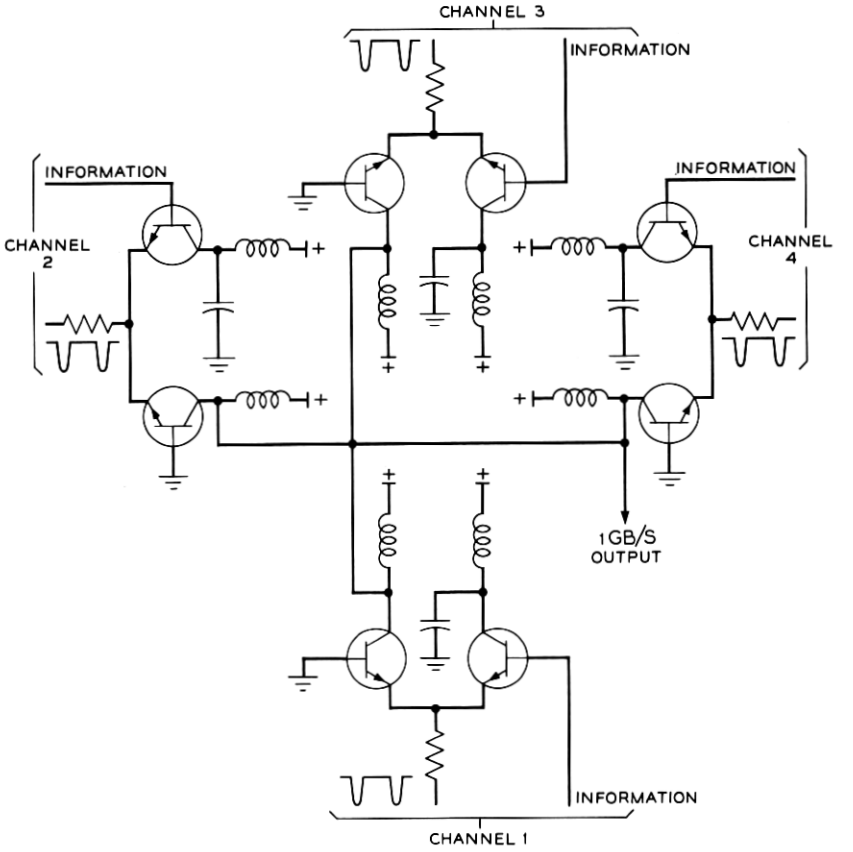

Fig. 22—Alternative realization of information gates and multiplexer functions.

collector output capacitance but present-day devices are available with values of capacitance significantly below a picofarad and time constants of less than 100 ps should easily be obtained.

With the previously described circuit elements, multilevel coding is readily implemented. This form of coding is achieved merely by supplying spike waveforms with the necessary quantization in amplitude levels. The system depicted in Fig. 23 is such a realization for a four-level coding scheme. Not shown is the conversion logic which is required at the inputs to the information gates but since this is at a relatively slow data rate (250 Mb/s) it is easily accomplished with standard integrated circuits. Multilevel PCM coding schemes are indeed attractive in view of the low system noise as will be discussed later.

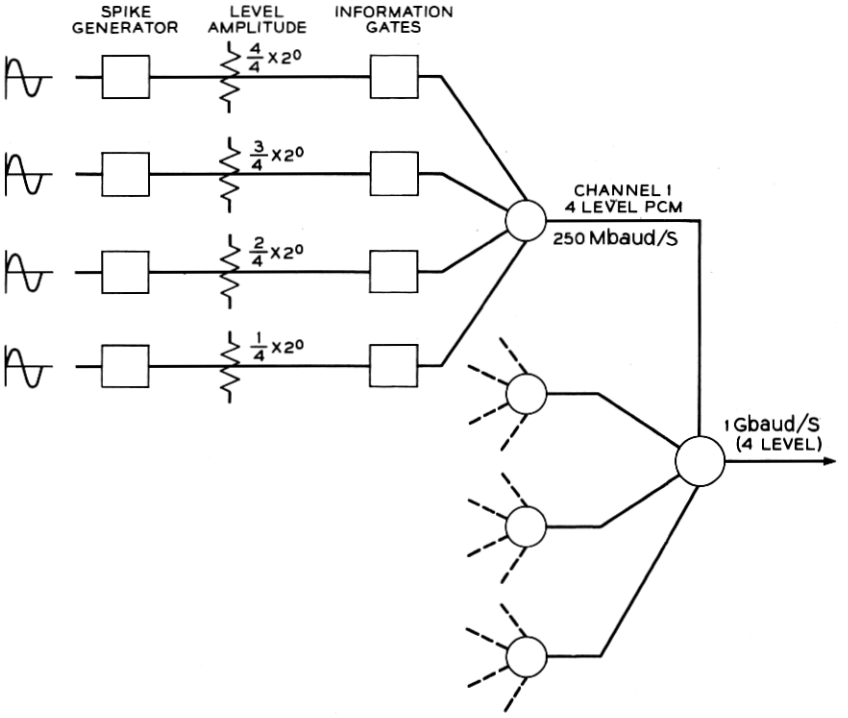

Fig. 23—Multilevel PCM coding schema.

VII. SYSTEM PERFORMANCE

The complete system was established in accordance with the basic schemas of Figs. 2 and 16. Optical loss and beam parameters are important factors in such systems where efficient use of beam power and optical component matching are required. Losses through passive optical components are relatively unimportant (typically 1 percent or less per surface). However, modulator losses are significant because of optical absorption and beam blockage due to large aspect ratio modulators. To achieve efficient optical matching, exact knowledge of the beam parameters is required; this was obtained by two experimental techniques, viz., slit measurements and edge measurements similar to those of Arnaud, et al.[50] Both techniques made possible reliable estimates of the beam intensity profile. Typical of these measurements is the experimentally obtained diffraction-limited waist pattern shown in Fig. 24 which compares well with the calculated waist pattern [from equation (14)] also presented. Such exact knowledge of beam parameters enabled modulator losses as low as 0.5 dB to be obtained. In practice, however, low-loss transmission does not coincide with high-efficiency modulation depths but, nevertheless, losses as low as a few decibels are obtainable.

Practically realizable system transfer function coefficients of approximately 0.17/W were obtained as opposed to 0.5/W predicted by equation (3). This lower value is accounted for primarily by the nonlinear modulation mode. Other factors, including reflection from the exiting face of the modulator crystal and analyzer losses, also reduce the coefficient. Nevertheless, output voltages of 20 mV result from applied modulation potentials of 4 V.

The total system performance at a bit rate of 1 Gb/s is illustrated in Fig. 25a. This output from the photodetector (lower trace) results from the impression of a 101101 word pattern on channel 1, channels 2 through 4 having all 1's impressed. This particular result is presented as typical of the many different word patterns that have been successfully transmitted over the laser beam. The detected electrical output from the photodetector after transmission via the beam is to be compared with the electrical modulation waveform exiting from the modulator structure (upper trace). Two points are to be noted, one the fidelity, and two, the low noise. The first point is indicative of

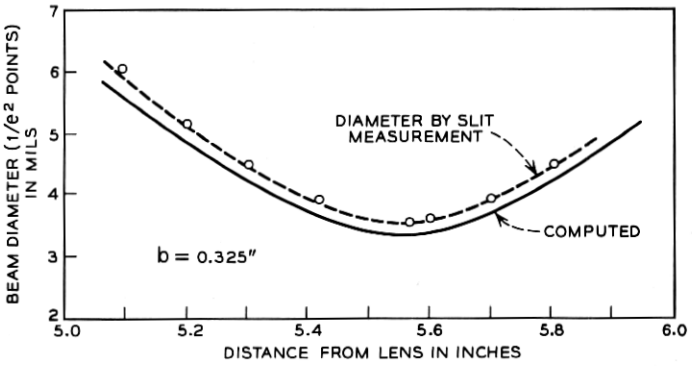

Fig. 24—Experimental and computed beam profiles at diffraction-limited waist.

the exceptionally wide bandwidth of the system while the latter augurs well for a multilevel type of coding.

The bandwidth of the system is mainly determined by the length of the modulator crystal and a length of 0.6 inch results in a frequency axis crossing point of approximately 5 GHz. This consequentially produces, in the time domain, a step response rise time of approximately 200 ps. Figure 25b is an experimentally observed response for a 250-ps rise time pulse excitation (upper trace); the detected pulse (lower trace) exhibits a rise time of approximately 400 ps which is commensurate with a system response time of 200 ps. The system bandwidth, of course, can be made arbitrarily large, up

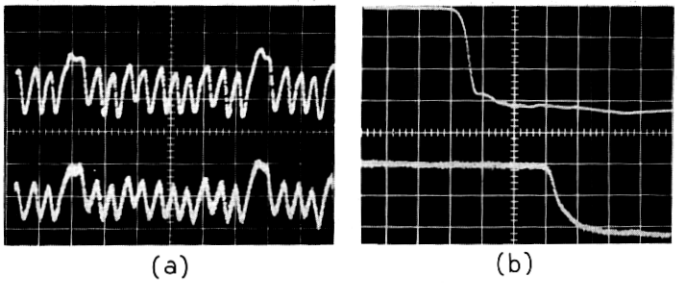

Fig. 25—(a) Upper trace: electrical modulation signal exiting from modulator (2 ns/cm, 2 V/cm); lower trace: detected optical signal after transmission over laser beam (2 ns/cm, 10 mV/cm). (b) Upper trace: applied electrical modulation waveform; lower trace: detected optical signal after transmission over laser beam (500 ps/cm).

to the limit of the photodetector, by reducing the length of the modulator crystal. This increase in bandwidth is paid for at the expense of smaller depths of modulation.

Some small deviations in waveform shape are observable between that exiting from the modulator crystal (Fig. 25a upper trace) and that shown in Fig. 21b for which there is a pure resistive driving point impedance. This is attributable to the slight impedance mismatch between the modulator structure and the transmission line structure in which it is embedded. Its primary cause is reflections in the traveling-wave modulator rather than coupling paths to the electronic circuits since no significant reflections are observed in this path for test waveforms. The effect, however, is not great and the overall result is that of widening the PCM eye pattern, which is a desirable feature.

The noise level observed in the waveform of Fig. 25a is attributable to a combination of the noise in the photodetector, that due to the laser beam, and that due to the sampling noise in the instrument used to observe the waveform. The latter source, which is intrinsically unrelated to the actual system, provides the dominant contribution. Nevertheless, taking the signal-to-noise ratio as the observed 20 dB, results in a possible system information rate in excess of 3 Gb/s in accordance with the Shannon-Hartley law. This information rate would require, of course, a more efficient coding scheme.

Long-term stability of the system is measured in hours. Loss of stability is due to the onset of mode competition resulting from etalon adjustment wandering, although it is not difficult to envisage a correction mechanism via a monitoring and servomechanism scheme to extend this time to arbitrarily long periods. The modulator crystal is not temperature controlled and ambient temperature variations will cause a loss of system bias point. As discussed earlier, this is readily rectified using a cascaded rod structure to achieve bias stabilization.

Once detected, the received signal may be demultiplexed conveniently by existing techniques. A suitable optical technique has been described by Kinsel[51] for demultiplexing two channels and a related technique for an arbitrarily large number of channels has been proposed by Chen.[52] Electronic techniques employing a sampling scheme are also applicable without placing severe constraints on the demultiplexer circuit. This relaxation in requirements results from the relatively small amplitudes of the detected waveform. In repeater applications, the demultiplexed pulses can be conveniently amplified in relatively

low-frequency amplifiers (250 Mb/s) in order to provide drive signals to subsequent information gates.

VIII. CONCLUSIONS

An optical communications system has been described which has a demonstrated information capacity of 1 Gb/s. The major difficulties to achieving high information rates have been outlined as lying in high-speed circuit realization and the interfacing of high-speed electronic circuits and optics. These difficulties have been alleviated by a system architecture and subsystem design which not only results in the high information rate described but shows promise for future systems of even higher rates. These higher rates could be achieved by a multiplexing of quantized electrical pulse amplitudes, and the possibility also exists for a further increase in rate with optical multiplexing.

The realization of the high-speed performance of the electronic circuits relies not only on the design configuration but heavily on the fabrication technology employed. In the case of the 1-Gb/s system a beam lead chip on alumina substrate technology has provided sufficiently low parasitic reactance values to achieve the desired speed performance. In a wholly electronic communications system, the circuits evolved in this study could find advantageous application in achieving data rates which are closer to the most efficient bandwidth utilization rate for coaxial systems.[53]

Transmission channels have not been considered in this paper; these channels could be of an open atmospheric, gas lens guide, or fiber optic type. Recent advances in low-loss fibers[54,55] make these look particularly attractive for optical transmission and efficient utilization of these fibers could call for wide bandwidth schemes of the type described.

Practical laser communications systems already are in use[14,56] and the exponential growth in bandwidth requirements will undoubtedly force a greater exploitation of the laser portions of the electromagnetic spectrum. Even the high information rates described nowhere near approach the theoretical bandwidth capabilities of optical communications systems. This ultimate limit will probably only be realized with improved optical processing of logic so that the potential of the extremely short pulses now available from such lasers as the neodymium YAG and the solid state GaAs forms can be realized.

IX. ACKNOWLEDGEMENTS

It is with pleasure that the author acknowledges all those who have contributed to this work and, in particular, H. J. Schulte and P. K. Runge for stimulating discussions, B. G. King and D. A. Hodges for their encouragement during the course of this work, M. R. Biazzo who mounted and tested the modulator crystals, H. Melchior who supplied the photodiodes, and last but not least G. M. Chin for his excellent technical assistance.

REFERENCES

1. Standley, R. D., "Performance of an 11 GHz Optical Modulator Using $LiTaO_3$," J. Appl. Opt., May 1971, pp. 1022–1023.
2. Melchior, H., and Lynch, W. T., "Signal and Noise Response of High Speed Germanium Avalanche Photodiodes," IEEE Trans. Elec. Devices, *ED-13,* No. 12 (December 1966), pp. 829–838.
3. Denton, R. T., Kinsel, T. S., and Chen, F. S., "224 Mc/s Optical Pulse Code Modulator," Proc. IEEE (Letters), *54,* October 1966, pp. 1472–1473.
4. Gordon, E. I., "A Review of Acoustic-optic Deflection in Modulation Devices," Appl. Opt., *5,* No. 10 (October 1966), pp. 1629–1639.
5. Zeeman, P., *Researches in Magneto-optic,* London: Macmillan and Co., Ltd., 1913.
6. Kaminow, I. P., and Turner, E. H., "Electrooptic Light Modulators," Appl. Opt., *5,* No. 10 (October 1966), pp. 1612–1628.
7. Pockels, F., *Lehrbuck Der Kristalloptik,* Leipzig: B. Teubner, 1906.
8. Kaminow, I. P., and Johnston, W. D., Jr., "Quantitative Determination of Sources of the Electro-optic Effect in $LiNbO_3$ and $LiTaO_3$," Phys. Rev., *160,* No. 3.
9. Ashkin, A., et al., "Optically-Induced Refractive Index Inhomogeneities in $LiNbO_3$ and $LiTaO_3$," Appl. Phys. Letters, *9,* No. 1 (July 1966), pp. 72–74.
10. Denton, R. T., Chen, F. S., and Ballman, A. A., "Lithium Tantalate Light Modulators," J. Appl. Phys., *38,* No. 4 (March 1967), pp. 1611–1617.
11. Smith, P. W., "Mode Locking of Lasers," Proc. IEEE, *58,* No. 9 (September 1970), pp. 1342–1357.
12. Kogelnik, H., and Patel, C. K. N., "Mode Suppression and Single Frequency Operation in Gaseous Optical Masers," Proc. IRE, *50,* No. 11 (November 1962).
13. Denton, R. T., and Kinsel, T. S., "Terminals for a High-Speed Optical Pulse Code Modulation Communications System: I. 224-Mbit/s Single Channel," Proc. IEEE, *56,* No. 2 (February 1968), pp. 140–145.
14. Masuda, T., Uchida, T., Ueno, Y., and Shimamura, T., "An Experimental High Speed PCM/AM Optical Communications System Using Mode-Locked HeNe Gas Lasers," IEEE Int. Conf. Commun., San Francisco, June 8–10, 1970.
15. Di Domenico, M., Jr., Geusic, J. E., Marcos, H. M., and Smith, R. G., "Generation of Ultrashort Optical Pulses by Mode Locking the YAlG:Nd Laser," Appl. Phys. Letters, *8,* No. 7 (April 1966), pp. 180–183.
16. Kinsel, T. S., and Denton, R. T., "Terminals for a High-Speed Optical Pulse Code Modulation Communications System: II. Optical Multiplexing and Demultiplexing," Proc. IEEE, *56,* No. 2 (February 1968), pp. 146–154.
17. Hirano, J., and Kimura, T., "Multiple Mode Locking of Lasers," IEEE J. Quantum Elec., *QE-5,* No. 5 (May 1969), pp. 219–225.

18. Runge, P., "Ein lm langer He-Ne-Laser für 0.63 μm mit nur einer einzigen Frequenz," Archiv der Elektrischen Übertragung, *19,* 1965, pp. 573–574.
19. Kinsel, T. S., "Wide-Band Optical Communication Systems: Part I—Time Division Multiplexing," Proc. IEEE, *58,* No. 10 (October 1970), pp. 1666–1683.
20. Hance, H. V., Peterson, D. G., Ward, R. B., and Ohlman, R. C., "A Laboratory Ultra-Wideband FM/IM Optical Data Relay System," IEEE Int. Conf. Commun. San Francisco, June 8–10, 1970.
21. Gabler, F., and Sokob, P., "Senarmont Compensator," Z. Instrumentenk., *58,* 1938, p. 301.
22. Poincaré, H., *Théorie Mathématique de la Lumiére,* Paris: Gauthiers-Villars, 1892.
23. Kogelnik, H., and Li, T., "Laser Beams and Resonators," Appl. Opt., *5,* No. 10 (October 1966), pp. 1550–1567.
24. Kogelnik, H., "Modes in Optical Resonators," *Lasers,* Vol. 1, Ed. A. K. Levine, New York: Marcel Dekker, Inc., 1966.
25. Bhawalkar, D. D., Goncharenko, A. M., and Smith, R. C., "Propagation of Gaussian Beams in Anisotropic Media," Brit. J. App. Phys., *18,* pp. 1431–1441.
26. Levinstein, H. J., et al., "Reduction of the Susceptability of Optically Induced Index Inhomogeneities in $LiTaO_3$ and $LiNbO_3$," J. Appl. Phys., *38,* No. 8 (July 1967), pp. 3101–3102.
27. Riesz, R. P., and Biazzo, M. R., "Gigahertz Optical Modulation," Appl. Opt., *8,* 1969, pp. 1393–1396.
28. Chow, K. K., Comstock, R. L., and Leonard, W. B., "1.5 GHz Bandwidth Light Modulator," IEEE J. Quantum Elec., *QE-5,* No. 12 (December 1969), pp. 618–620.
29. Rigrod, W. W., and Kaminow, I. P., "Wideband Light Modulation," Proc. IEEE, *51,* No. 1 (January 1963), pp. 1–4.
30. Bicknell, W. E., Yap, B. K., and Peters, C. J., "0 to 3 GHz Traveling-Wave Electro-optic Modulator," Proc. IEEE, *55,* No. 2 (February 1967), pp. 225–226.
31. Di Domenico, M., Jr., and Anderson, L. K., "Broadband Electro-optic Traveling-Wave Light Modulators," B.S.T.J., *42,* No. 6 (November 1963), pp. 2621–2678.
32. Grover, F. W., *Inductance Calculations, Working Formulas and Tables,* New York: Dover Publications, Inc., 1946.
33. Spencer, E. G., Lenzo, P. V., and Ballman, A. A., "Dielectric Materials for Electro-optic, Elasto-optic and Ultrasonic Device Applications," Proc. IEEE, *55,* No. 12 (December 1967), pp. 2074–2108.
34. Kaminow, I. P., and Sharpless, W. M., "Performance of $LiTaO_3$ and $LiNbO_3$ Light Modulators at 4 GHz," Appl. Opt. *6,* 1967, p. 351.
35. Kaminow, I. P., Kompfner, R., and Louisell, W. H., "Improvements in Light Modulators of the Traveling-Wave Type," IRE Trans. on Microwave Theory and Techniques, *MTT-10,* No. 5 (September 1962).
36. Kaminow, I. P., and Liu, J., "Propagation Characteristics of Partially Loaded Two-Conductor Transmission Line for Broadband Light Modulators," Proc. IEEE, *51,* No. 1 (January 1963), pp. 132–136.
37. Peters, C. J., "Gigacycle Bandwidth Coherent Light Traveling-Wave Phase Modulator," Proc. IEEE, *51,* No. 1 (January 1963), pp. 147–152.
38. Nelson, D. F., and Turner, E. H., "Electro-optic and Piezo-electric Coefficients and Refractive Index of Gallium Phosphide," J. Appl. Phys., *39,* No. 7 (June 1968), pp. 3337–3343.
39. Bond, W. L., "Measurement of the Refractive Indices of Several Crystals," J. Appl. Phys., *36,* No. 2 (May 1965), pp. 1674–1677.
40. Kaminow, I. P., "Microwave Modulation of the Electro-optic Effect in KH_2PO_4," Phys. Rev. Letters *6,* No. 10 (May 1961), pp. 528–530.
41. Peters, C. J., "Traveling Wave Amplitude Modulator," NEREM Record 1964, November 1964, pp. 70–71.
42. Peters, C. J., "Gigacycle-Bandwidth Coherent-Light Traveling Wave Amplitude Modulator," Proc. IEEE, *53,* No. 5 (May 1965), pp. 455–460.

43. Biazzo, M. R., "Fabrication of a Lithium Tantalate Temperature Stabilized Optical Modulator," Appl. Opt., *10,* No. 5 (May 1971).
44. Friis, H., "Analysis of Harmonic Generator Circuits for Step Recovery Diodes," Proc. IEEE, *55,* No. 7 (July 1967), pp. 1192–1194.
45. Dietrich, A. F., and Goodall, W. M., "Solid State Generator for 2×10^{-11} Second Pulses," Proc. IRE (Correspondence), *48,* 1960, pp. 791–792.
46. Gray, P. E., et al., *Physical Electronics and Circuit Properties of Transistors,* New York: John Wiley and Sons, 1964.
47. Kirk, C. T., Jr., "A Theory of Transistor Cut-off Frequency (f_T) Fall-off at High Current Density," IEEE Trans. Elec. Devices, *ED-9,* No. 2 (March 1962), pp. 164–173.
48. Lepselter, M. P., and Sze, S. M., "Silicon Schottky Barrier Diode with Near-Ideal I-V Characteristics," B.S.T.J., *47,* No. 2 (February 1968), pp. 195–208.
49. Mead, C. A., "Metal-Semiconductor Surface Barriers," Solid State Elec., *9,* 1966, pp. 1023–1033.
50. Arnaud, J. A., Franke, E. A., Hubbard, W. M., Mandeville, G D., de la Claviere, B., and Franke, J. M., "Technique for Fast Measurement of Gaussian-Beam Parameters," J. Opt. Soc. Am., *60,* No. 5 (May 1970), p. 739.
51. Kinsel, T. S., "Lightwave of the Future: Optical PCM," Electronics, September 16, 1968, pp. 123–128.
52. Chen, F. S., "Demultiplexers for High-Speed Optical PCM," IEEE J. Quantum Elec., *QE-7,* No. 1 (January 1971), pp. 24–29.
53. Freeny, S. L., and Chang, R. W., "Hybrid Digital Transmission Systems—Part 2: Information Rate of Hybrid Coaxial Cable Systems," B.S.T.J., *47,* No. 8 (October 1968), pp. 1687–1711.
54. Kapron, F. P., Keck, D. B., and Maurer, R. D., "Radiation Losses in Glass Optical waveguides," IEE Conf. Trunk Telecommunications by Guided Waves, September 20, 1970, London, p. 29.
55. Kapron, F. P., Keck, D. B., and Maurer, R. D., "Radiation Losses in Glass Optical Waveguides," Appl. Phys. Letters, *77,* November 15, 1970, p. 423.
56. IEEE Spectrum, *7,* No. 6 (June 1970), p. 120.